Coherent Spin Dynamics of Electrons and Holes in CsPbBr 3 Colloidal Nanocrystals

Philipp S Grigoryev, Vasilii V Belykh, Dmitri R Yakovlev, Emmanuel Lhuillier, Manfred Bayer

NANO LETTERS

pubs.acs.org/NanoLett Letter

Coherent Spin Dynamics of Electrons and Holes in $CsPbBr_3$ Colloidal Nanocrystals

Philipp S. Grigoryev, Vasilii V. Belykh, Dmitri R. Yakovlev,* Emmanuel Lhuillier, and Manfred Bayer

Cite This: https://doi.org/10.1021/acs.nanolett.1c03292 Read Online

ACCESS | Metrics & More | Article Recommendations | Supporting Information

ABSTRACT: The spin dynamics in $CsPbBr_3$ lead halide perovskite nanocrystals are studied by picosecond pump−probe Faraday rotation in an external magnetic field. Coherent Larmor precession of electrons and holes with spin dephasing times of ∼600 ps is detected in a transversal magnetic field. The longitudinal spin relaxation time in weak magnetic fields reaches 80 ns at a temperature of 5 K. In this regime, the carrier spin dynamics is governed by nuclear spin fluctuations characterized by an effective hyperfine field strength of 25 mT. The Landé factors determining the carrier Zeeman splittings are g_e = +1.73 for electrons and g_h = +0.83 for holes. A comparison with a $CsPbBr_3$ polycrystalline film and bulk single crystals evidences that the spatial confinement of electrons and holes in the nanocrystals only slightly affects their g factors and spin dynamics.

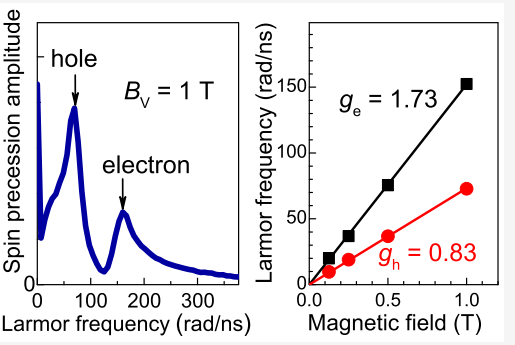

KEYWORDS: *Perovskite nanocrystals, $CsPbBr_3$, coherent spin dynamics, electron and hole g-factors, pump−probe time-resolved Faraday rotation*

Lead halide perovskite nanocrystals (NCs) have only quite recently joined the rich family of semiconductor NCs grown by colloidal synthesis.[1−6] They show a remarkable quantum yield up to 90% even for bare NCs, as surface states do not act detrimentally on the exciton emission efficiency. In these materials, the energies of surface states and of defects and impurities are not located within the band gap, which strongly suppresses channels for the nonradiative recombination of optical excitations in the vicinity of the band gap. This known phenomenon of the perovskites is often summed up as a defect-tolerant band structure. The inorganic lead halide perovskites $CsPbX_3$ (X = I, Br, or Cl) allow one to tune the band gap across a wide spectral range from the infrared up the ultraviolet by mixing the halogen composition. Further flexibility in NC band-gap tuning arises from the quantum confinement of the charge carriers, whereby details of the exciton fine structure are governed by the shape and size of the NC.[7−10] Simple fabrication, a high quantum yield, and tunable optical properties also make lead halide perovskite NCs promising materials for spintronics applications. Still, only a few studies have been performed so far in this field. In particular, neutral and charged excitons in single NCs were identified by their Zeeman splitting in magnetic fields,[11] and the importance of the Rashba effect was elaborated.[12] Strong magnetic fields of 30 T allowed one to identify the influence of negatively charged excitons (trions) and dark excitons on the optical properties of NC ensemble.[13] Anisotropic exciton Zeeman splitting in magnetic field was observed,[14] the coherent spin dynamics of holes were explored in $CsPbBr_3$ NCs,[15] and the picosecond spin dynamics of carriers were reported in $CsPbI_3$ NCs.[16]

To understand and interpret spin-dependent phenomena, precise knowledge of the values and signs of the charge-carrier g-factors is of key importance. Also, the characteristic time scales of the spin dynamics (longitudinal spin relaxation time, T_1, spin coherence time, T_2, and ensemble spin dephasing time, T_2^*) are needed. It is important that these parameters are measured directly and preferably on the same samples. Even for bulk lead halide perovskites, the published information is still fragmentary, often providing controversial conclusions.[17−25]

Time-resolved pump−probe Faraday/Kerr rotation is an established technique for fulfilling the previously defined conditions for comprehensive spin physics studies of semiconductors,[26,27] as it provides direct access to g-factors and the spin relaxation times. For example, it was successfully applied to colloidal II−VI semiconductor NCs.[28−31] Furthermore, its potential was recently demonstrated for $CsPbBr_3$ single crystals[32] and NCs[15] and for $CH_3NH_3PbCl_xI_{3-x}$ polycrystalline films.[33]

Received: August 24, 2021
Revised: September 27, 2021

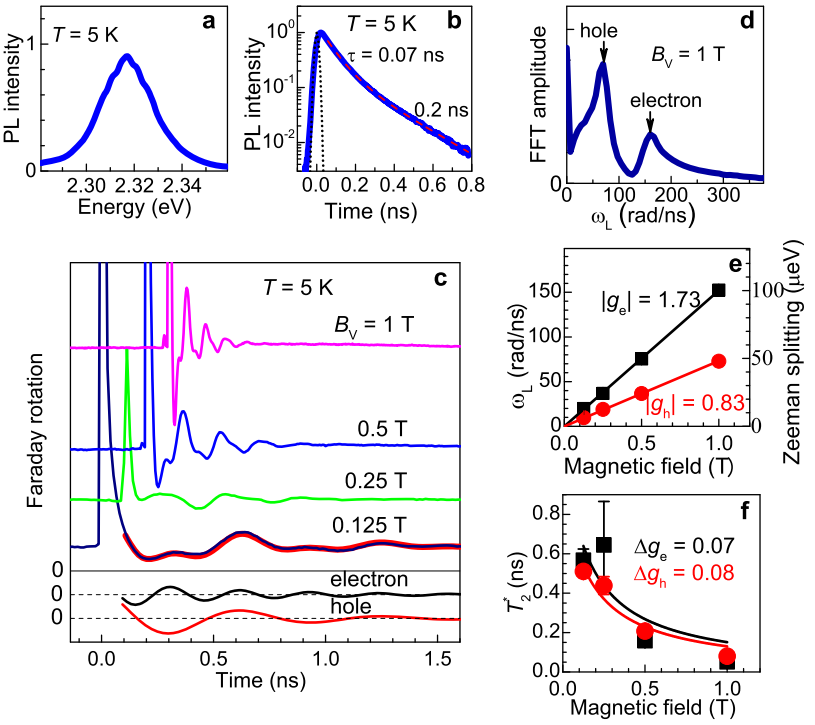

Figure 1. (a) Photoluminescence spectrum of $CsPbBr_3$ NCs. (b) Time-resolved recombination dynamics measured at the maximum of the PL line. The black dotted line shows the instrumental response function, whereas the red dashed line shows the double-exponential fit. (c) Coherent spin dynamics measured at 2.330 eV in different magnetic fields applied in Voigt geometry. The curves are shifted vertically and horizontally for clarity. The thick red line is a fit to the data at $B_V = 0.125$ T with eq 1 and $S_e/S_h = 0.5$. In the bottom, the black and red lines are the two components of the fit describing the electron and hole spin precession. (d) Fast Fourier transform (FFT) spectrum of the Faraday rotation dynamics at $B_V = 1$ T. (e) Magnetic field dependencies of the Larmor precession frequencies (corresponding Zeeman splittings are shown on the right axis) for electrons and holes. The error bars are within the data points. Solid lines are linear fits, giving $|g_e| = 1.73$ and $|g_h| = 0.83$. (f) Magnetic field dependencies of the spin dephasing times for electrons and holes. Lines are fits according to eq 2, with parameters given in the text.

In this Letter, we investigate the coherent spin dynamics of electrons and holes in $CsPbBr_3$ NCs using time-resolved pump−probe Faraday rotation (ppFR). We measure the electron and hole *g*-factors, their spread within the NCs ensemble, and the temperature dependence of the transverse and longitudinal spin relaxation times. The carrier interaction with the nuclear spins and its role in the spin dynamics are studied. The spin dynamic parameters in $CsPbBr_3$ NCs are compared with those in a polycrystalline film and a bulk single crystal.

OPTICAL PROPERTIES OF NANOCRYSTALS

We study $CsPbBr_3$ NCs dispersed in polymethyl methacrylate (PMMA) and spin-coated on a glass coverslip. (For synthesis details, see Section S2 in the Supporting Information.) The NCs have a cubic shape with a typical size of 10 nm, which slightly exceeds the exciton Bohr diameter of 7 nm. Therefore, the excitons experience a rather weak size quantization. Transmission electron microscopy images and optical spectra of similar $CsPbBr_3$ NCs can be found in ref 13. It should be noted that whereas $CsPbBr_3$ NCs are known to crystallize in the cubic phase,[3] a recent report shows that they can exhibit tetragonal and orthorhombic phases at cryogenic temperatures.[11] Lower crystal symmetry will likely result in an anisotropy of the charge-carrier *g*-factors.

To characterize the optical properties of the studied $CsPbBr_3$ NCs, we measured the photoluminescence (PL) spectrum and recombination dynamics at a temperature of $T =$ 5 K; see Figure 1a,b. The results are typical for $CsPbBr_3$ NCs, as reported in literature; see, for example, ref 13 and references therein. The PL line has maximum at 2.317 eV and a full width at half-maximum of 29 meV. It shows a fast recombination, two-component dynamics with a decay of 0.07 and 0.2 ns (Figure 1b), in line with the 0.2 ns decay measured in single NC experiments.[11] We have checked that the application of the magnetic field up to 6 T only slightly elongates the PL decay. These decay times are considerably shorter than the exciton decay time of 0.9 ns in $CsPbBr_3$ bulk crystals.[32] In general, the emission of an NC ensemble can be contributed by neutral and charged NCs. Therefore, the PL can contain the emission of neutral, negatively charged, and positively charged excitons. The ratio of their populations depends on the synthesis protocol, the sample preparation, and the optical excitation conditions. In our previous study,[13] we measured polarized PL and recombination dynamics in high magnetic fields up to 30 T of similar $CsPbBr_3$ NCs and concluded that at liquid helium temperatures, the emission is mainly contributed by negatively charged excitons with some contribution from neutral excitons. The present study using the ppFR technique[27] allows us to gain more information on the NC charging,[30] as will be discussed as follows.

COHERENT SPIN DYNAMICS OF ELECTRONS AND HOLES IN NANOCRYSTALS

To address the carrier spin dynamics, we use ppFR; see the Methods in the Supporting Information. Here circularly polarized pump pulses optically induce a carrier spin

https://doi.org/10.1021/acs.nanolett.1c03292
Nano Lett. XXXX, XXX, XXX−XXX

polarization, while the linearly polarized probe pulses detect its time evolution by varying their delay relative to the pump.

Figure 1c shows the spin dynamics measured for different magnetic fields applied in the Voigt geometry (field orientation perpendicular to the collinear pump and probe beams). The Faraday rotation amplitude oscillates with time, reflecting the coherent spin precession at the Larmor frequency about the magnetic field. The precession frequency increases with magnetic field strength, B_V, growing from 0.125 to 1 T. Simultaneously, the signal decay accelerates. The modulations in the oscillatory signal arise from the contribution of two components with different precession frequencies, as confirmed in the fast Fourier transform (FFT) spectrum of the dynamics in Figure 1d. Indeed, the Faraday rotation dynamics can be well-fitted by the sum of two exponentially decaying oscillations

$$A_{FR} = S_e \cos(\omega_{L,e}t)\exp(-t/T^*_{2,e}) + S_h \cos(\omega_{L,h}t)\exp(-t/T^*_{2,h}) \quad (1)$$

Here $S_{e(h)}$ is the amplitude of the electron (hole) spin signal, $\omega_{L,e(h)}$ is the Larmor precession frequency of electrons (holes), and $T^*_{2,e(h)}$ is the electron (hole) spin dephasing time. The contributions of the two dynamics components at $B_V = 0.125$ T are shown separately in the bottom of Figure 1c. The fit gives $T^*_{2,e} \approx 0.6$ ns and $T^*_{2,h} \approx 0.5$ ns with comparable amplitudes of the electron and hole signals, $S_e/S_h \approx 0.5$. The Larmor precession frequencies of both components increase linearly with magnetic field (Figure 1e). By fitting them with $\omega_{L,e(h)} = |g_{e(h)}|\mu_B B_V/\hbar$, where μ_B is the Bohr magneton and $g_{e(h)}$ is the electron (hole) g factor, we evaluate $|g_e| = 1.73$ and $|g_h| = 0.83$.

We attribute the high-frequency component with the g-factor of 1.73 to the electron and the low-frequency component with the g-factor of 0.83 to the hole by analogy to bulk $CsPbBr_3$ perovskites.[32] Note that our experimental technique is not sensitive to the g-factor sign, which should be determined using an alternate method. We use here the knowledge of the exciton g-factor, $g_X = +2.4$, that we measured in $CsPbBr_3$ NCs,[13] and the fact that in lead halide perovskites, $g_X = g_e + g_h$. This allows us to conclude that in the studied NCs, both electron and hole g-factors are positive, similar to $CsPbBr_3$ bulk crystals;[32] for details see Section S4 in the Supporting Information.

Let us clarify now the important question of whether neutral or singly charged NCs are responsible for the ppFR signal. In the case of neutral NCs, the signal should originate from the photogenerated electrons and holes bound to neutral excitons. There are two arguments that let us exclude this neutral exciton scenario. First, the measured spin dynamics should then be limited by the exciton recombination time, which is 0.2 ns for the studied NCs (Figure 1b). The measured spin dephasing times of electrons (0.6 ns) and holes (0.5 ns) are much longer than the exciton recombination time. The second argument is related to the exciton fine structure. Magneto-optical studies of emission from single $CsPbBr_3$ NCs show that the zero-field exciton exchange splitting of neutral excitons is ~0.6 meV[11] and that most NCs at low temperatures have either tetragonal or orthorhombic crystal symmetry. Note that in rather similar $FAPbBr_3$ NCs the splitting is found to be in the range from 0.3 to 1.7 meV.[10] The exciton exchange interaction couples electron and hole spin so that the spins of the electrons and holes forming the exciton do not precess independently. This becomes possible only in strong magnetic fields where the carrier Zeeman splitting exceeds the exchange energy and the spin coupling is broken. One can see from the right scale of Figure 1e that in the studied NCs, we detect electron and hole spin precession in the low field regime with Zeeman splittings of ~0.01 meV, that is, much smaller than the neutral exciton exchange splitting. We conclude that neutral NCs (i.e., neutral excitons) cannot contribute notably to the coherent spin dynamics measured in the ppFR experiment. Note that this conclusion contradicts the one of ref 15 that the measured hole spin beats can be associated with a hole bound to an exciton.

In NCs charged by either a single electron or a single hole, the ppFR signal is contributed by the spin dynamics of these resident carriers, limited only by their spin relaxation times. The spin coherence of the resident carriers is generated via photoexcitation of a charge exciton (trion) state, as studied in great detail for (In,Ga)As/GaAs epitaxially grown quantum dots.[27,34] The exchange splitting is canceled in the trion and obviously also cannot occur for the resident carrier left in an NC after trion recombination. Therefore, the magnetic field dependence of the Larmor precession frequency is expected to be linear with zero energy offset at zero magnetic field. This is exactly what we find in the experiment in Figure 1e for both electrons and holes. On the basis of these arguments, we can safely conclude that the ppFR signals originate from singly charged NCs, both positively and negatively charged. From $S_e/S_h \approx 0.5$, we suggest that the fractions of negatively and positively charged NCs are comparable, with some preference for the positively charged NCs. It was shown that in $CsPbBr_3$ and $FAPbBr_3$ NCs photocharging results in negative and positive loading of the NCs.[35,36] This is consistent with the Fermi level being close to the midpoint of the gap in Cs and FA lead halide NCs, as demonstrated by photoemission spectroscopy.[37,38]

The spin dephasing times, of both electrons and holes, show strong magnetic field dependences; see Figure 1f. The dynamics shorten from 0.6 to 0.05 ns for electrons and from 0.5 to 0.08 ns for holes with increasing field up to 1 T. This decrease is provided by the spin dephasing in the ensembles with a dispersion of the g-factors, which translates to a spread of the Larmor precession frequencies. It is described by the following equation

$$\frac{1}{T^*_{2,e(h)}(B_V)} = \frac{1}{T^*_{2,e(h)}(0)} + \frac{\Delta g_{e(h)}\mu_B B_V}{\hbar} \quad (2)$$

Here $\Delta g_{e(h)}$ is the dispersion of electron (hole) g-factors. $T^*_{2,e(h)}(0)$ is the spin dephasing time at zero magnetic field, which is limited by the spin coherence time, $T_{2,e(h)}$, of the individual carriers and the spin relaxation mechanisms not related to the g-factor dispersion, for example, the hyperfine interaction with nuclear spin fluctuations. This equation gives reasonable fits to the experimental dependencies of $T^*_{2,e(h)}(B_V)$ with $T^*_{2,e}(0) = 1.2$ ns and $T^*_{2,h}(0) = 1.0$ ns and g-factor spreads of $\Delta g_e = 0.07$ and $\Delta g_h = 0.08$. Note that the measured g-factor spreads are about two times larger than those in bulk $CsPbBr_3$ single crystals.[32] This may be related to the spread of NC sizes and shapes, which determines the g factor and its anisotropy.

https://doi.org/10.1021/acs.nanolett.1c03292
Nano Lett. XXXX, XXX, XXX−XXX

Oscillating signals in the Faraday rotation dynamics are detectable up to temperatures of 35 K, as shown in Figure 2.

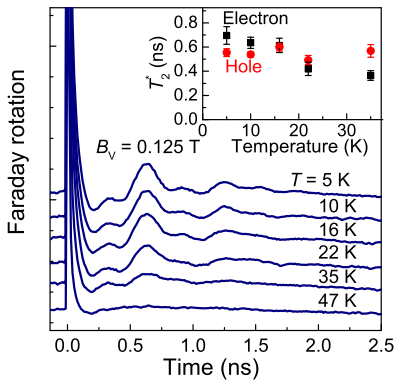

Figure 2. Dynamics of Faraday rotation signal in $CsPbBr_3$ NCs measured at 2.330 eV for different temperatures in B_V = 0.125 T. Data are shifted vertically for clarity. The inset shows the temperature dependence of the spin dephasing time for electrons and holes.

The amplitudes of both the electron and hole spin signals gradually decrease with increasing temperature. That means that the decrease in the signal amplitude is provided by a decreasing efficiency of the optical spin polarization. On the contrary, the spin dephasing times, shown in the inset of Figure 2, change only weakly in this temperature range. The hole dephasing time remains almost constant at $T_{2,h}^* = 0.5$ ns, whereas the electron time, $T_{2,e}^*$, slightly decreases from 0.7 to 0.4 ns. This is in contrast with the strong temperature dependence of $T_{2,e}^*$ in bulk $CsPbBr_3$,[32] where temperature induces the delocalization of carriers and the activation of spin relaxation mechanisms related to the spin−orbit coupling. On the contrary, in NCs, carriers are localized at any temperature. The other difference in NCs from bulk $CsPbBr_3$, presumably related to the localization, is the much more homogeneous spin dynamics for NCs (dephasing times and ratio between electron and hole contributions) for different positions on the sample.

LONGITUDINAL SPIN RELAXATION OF CARRIERS IN NANOCRYSTALS

Let us turn to experiments in the Faraday geometry where the external magnetic field, B_F, is applied along the light wave vectors. Consequently, the optically induced spin polarization of carriers along the field direction does not show Larmor precession. This allows one to measure the longitudinal spin relaxation time, T_1, and gather information on the nuclear spin fluctuations.

The magnetic field dependence of the Faraday rotation signal measured at a negative time delay of −1 ns is shown in Figure 3a. The finite signal amplitude implies that the spin relaxation time of carriers exceeds the repetition period of the laser pulses, T_R = 13.1 ns. In fact, as we will show, it exceeds several T_R periods and corresponds to a cumulative effect due to repeated pulse application. In this experiment, the laser helicity is kept constant, but the laser intensity is modulated with frequencies in the f = 0.3−6 MHz range. One can see that at the low modulation frequency of 0.3 MHz (black line), the signal amplitude has a minimum at zero magnetic field and increases with the field increase. It thus corresponds to a so-called polarization recovery curve (PRC).[39] The half width at half-maximum of the PRC equals 25 mT, which is the characteristic field of nuclear spin fluctuations acting on the carriers via the hyperfine interaction. In our recent study of $CsPbBr_3$ crystals, we showed experimentally and theoretically that in lead halide perovskites, the holes in the valence band have a considerably stronger hyperfine interaction compared with the conduction band electrons.[32] Therefore, we suggest that the PRC signal in $CsPbBr_3$ NCs is mainly contributed by the hole−nuclear hyperfine interaction.

When the pump modulation frequency is increased to 6 MHz, the PRC amplitude decreases; see Figure 3a. This is evidence that the modulation period, $1/f$, is comparable to T_1 in this case, and the spin accumulation loses its efficiency. Therefore, we used the spin inertia method to measure the spin relaxation time, T_1, in the longitudinal magnetic field.[32,39,40] In addition, the detected signal is retarded by the phase, ϕ, which we also measure; see the Methods in the Supporting Information for details. Figure 3b shows the PRC amplitude and tan ϕ as a function of the modulation frequency, which gives us two ways to evaluate T_1. Fitting the frequency dependence of the PRC amplitude with the spin inertia equation (Section S3 in the Supporting Information), we obtain T_1 = 83 ± 9 ns. The fit of the tan ϕ dependence on f with a linear equation (Section S4 in the Supporting Information) gives T_1 = 56 ± 5 ns. This difference in T_1 is caused by the nonmonoexponential spin relaxation dynamics: The amplitude of the spin polarization is more sensitive to the slow component in the dynamics, whereas the retardation phase is more dependent on the fast component. We note that

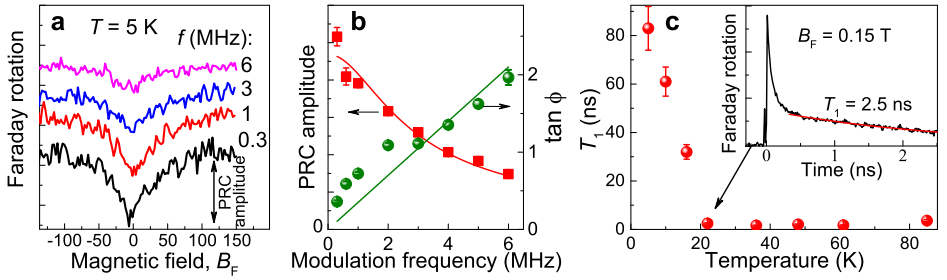

Figure 3. Spin dynamics of $CsPbBr_3$ NCs measured in longitudinal magnetic fields (Faraday geometry). (a) Polarization recovery curves measured at different pump modulation frequencies. Data are shifted vertically for clarity. T = 5 K. (b) PRC amplitude (red squares) and tangent of the retardation phase (green circles) as a function of the modulation frequency. Lines show fits with eqs S3 and S4 in the Supporting Information to the experimental data. T = 5 K. (c) Temperature dependence of the longitudinal spin relaxation time, T_1. Inset shows the Faraday rotation signal dynamics in the longitudinal magnetic field, B_F = 0.15 T, at T = 22 K.

https://doi.org/10.1021/acs.nanolett.1c03292
Nano Lett. XXXX, XXX, XXX−XXX

Table 1. Spin Parameters Measured for Different $CsPbBr_3$ Perovskite Samples[a]

	nanocrystals	polycrystalline film	bulk[32]
electron g-factor, g_e	+1.73	+1.78	+1.96
hole g-factor, g_h	+0.83	+0.77	+0.75
exciton g-factor, g_X	+2.4[13]		+2.35
electron spin dephasing time, $T_{2,e}^*$	0.6−0.7 ns	0.25 ns	0.9−5.2 ns
hole spin dephasing time, $T_{2,h}^*$	0.5 ns	0.4 ns	0.7−1.9 ns
longitudinal spin relaxation time, T_1	56−83 ns		32−53 ns

[a]Results for bulk $CsPbBr_3$ (single crystal) are taken from ref 32. T_2^* values in NCs and bulk are given for B_V = 0.125 T, and those in film are given for B_V = 0.25 T.

the evaluated T_1 values for NCs are a few tens of nanoseconds longer than T_1 for the corresponding bulk perovskites;[32] see Table 1.

The longitudinal spin relaxation time, T_1, determined from the frequency dependence of the PRC amplitude is shown in Figure 3c as a function of temperature. It rapidly decreases with temperature and saturates at ∼2 ns above 20 K. At temperatures higher than 20 K, T_1 was measured by fitting the decay of the Faraday rotation signal with a single exponential function; see the inset of Figure 3c.

COHERENT SPIN DYNAMICS IN POLYCRYSTALLINE FILM

We also studied the coherent spin dynamics in a $CsPbBr_3$ polycrystalline film. Its PL spectrum (Figure 4a) has an

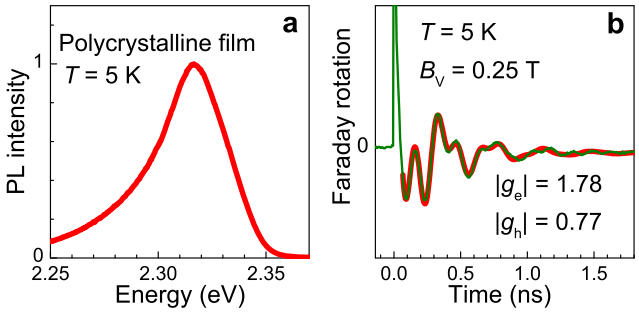

Figure 4. (a) Photoluminescence spectrum of the $CsPbBr_3$ polycrystalline film. (b) Coherent spin dynamics measured in the film at 2.330 eV for B_V = 0.25 T. The panel gives experimental data (green line) and fit to the data (red line) with eq 1 and S_e/S_h = 0.75.

asymmetric shape with a low-energy tail, similar to the low-temperature emission of bulk $CsPbBr_3$.[32] The spin precession monitored by ppFR is given in Figure 4b at B_V = 0.25 T and T = 5 K. Similar to the NCs, it contains two Larmor precession frequencies, where a fit with eq 1 gives the following parameters: $|g_e|$ = 1.78, $|g_h|$ = 0.77, $T_{2,e}^*$ = 0.25 ns, and $T_{2,h}^*$ = 0.4 ns. It is reasonable to suggest that similar to $CsPbBr_3$ bulk and NCs, $g_e > 0$ and $g_h > 0$ in the film.

SUMMARY OF g-FACTORS AND SPIN RELAXATION TIMES IN $CsPbBr_3$ PEROVSKITE STRUCTURES

It is instructive to compare the g-factor values for $CsPbBr_3$ perovskite NCs, polycrystalline film, and bulk crystals (Table 1). We note a small but monotonic variation of the g-factors when going from NCs to film and further to bulk. The rather close g-factor values are related to the weak quantum confinement in the studied NCs, which is also confirmed by their close energy positions of the PL emission. The behavior is in line with the well-known relation between the optical transition energy and the electron g-factor for semiconductors.[41−43] The small effect of confinement on the spin properties of the compared samples is further confirmed by the similar range of spin relaxation times in NCs and bulk perovskites.[32]

In conclusion, we performed a detailed study of the electron and hole spin dynamics in $CsPbBr_3$ perovskite NCs. Electron and hole g-factors of +1.73 and +0.83, respectively, have been measured from spin beats in the transverse magnetic field. The spin dephasing times T_2^* of ∼1 ns considerably exceed the exciton recombination time, which has allowed us to attribute the measured spin dynamics to NCs singly charged with an electron or a hole. In the longitudinal magnetic field, a spin relaxation time T_1 exceeding 80 ns has been measured. The influence of the carrier−nuclear hyperfine interaction, which controls the carrier spin dynamics at zero and weak magnetic fields, has been identified. Our study underlines that perovskite NCs have promising spin-dependent properties, very much comparable to the comprehensively studied epitaxially grown III−V quantum dots and colloidally synthesized II−VI NCs.

ASSOCIATED CONTENT

Supporting Information

The Supporting Information is available free of charge at https://pubs.acs.org/doi/10.1021/acs.nanolett.1c03292.

Details of experimental methods, synthesis and characterization of $CsPbBr_3$ NCs and polycrystalline film, and Zeeman Hamiltonian and g-factors of charge carriers and excitons (PDF)

AUTHOR INFORMATION

Corresponding Author

Dmitri R. Yakovlev − *Experimentelle Physik 2, Technische Universität Dortmund, 44221 Dortmund, Germany; P.N. Lebedev Physical Institute, Russian Academy of Sciences, 119991 Moscow, Russia; Ioffe Institute, Russian Academy of Sciences, 194021 St. Petersburg, Russia;* orcid.org/0000-0001-7349-2745; Email: dmitri.yakovlev@tu-dortmund.de

Authors

Philipp S. Grigoryev − *Spin Optics Laboratory, St. Petersburg State University, 199034 St. Petersburg, Russia;* orcid.org/0000-0002-3349-062X

Vasilii V. Belykh − *Experimentelle Physik 2, Technische Universität Dortmund, 44221 Dortmund, Germany; P.N. Lebedev Physical Institute, Russian Academy of Sciences, 119991 Moscow, Russia;* orcid.org/0000-0002-0032-748X

https://doi.org/10.1021/acs.nanolett.1c03292
Nano Lett. XXXX, XXX, XXX−XXX

Emmanuel Lhuillier − *Sorbonne Université, CNRS, Institut des NanoSciences de Paris, INSP, 75005 Paris, France;* orcid.org/0000-0003-2582-1422

Manfred Bayer − *Experimentelle Physik 2, Technische Universität Dortmund, 44221 Dortmund, Germany; Ioffe Institute, Russian Academy of Sciences, 194021 St. Petersburg, Russia;* orcid.org/0000-0002-0893-5949

Complete contact information is available at: https://pubs.acs.org/10.1021/acs.nanolett.1c03292

Notes

The authors declare no competing financial interest.

■ ACKNOWLEDGMENTS

We thank M. M. Glazov, A. V. Rodina, and Al. L. Efros for fruitful discussions. We acknowledge financial support by the Deutsche Forschungsgemeinschaft via the SPP2196 Priority Programme (Project YA 65/26-1) and the International Collaborative Research Centre TRR160 (Project B1). The research of V.V.B. and partially of D.R.Y. was supported by the Government of the Russian Federation (contract no. 075-15-2021-598 at the P.N. Lebedev Physical Institute). P.S.G. acknowledges St. Petersburg State University for a research grant 73031758. E.L. acknowledges the support of the ERC starting grant blackQD (grant no. 756225) of the French state funds managed by the ANR within the Investissements d'Avenir programme under reference ANR-11-IDEX-0004-02 and, more specifically, within the framework of the Cluster of Excellence MATISSE and by grant IPER-Nano2 (ANR-18CE30-0023-01). M.B. acknowledges support by the Mercur Foundation (grant Pe-2019-0022).

■ REFERENCES

(1) Kovalenko, M. V.; Protesescu, L.; Bodnarchuk, M. I. Properties and potential optoelectronic applications of lead halide perovskite nanocrystals. *Science* **2017**, *358*, 745−750.

(2) Chen, Q.; Wu, J.; Ou, X.; Huang, B.; Almutlaq, J.; Zhumekenov, A. A.; Guan, X.; Han, S.; Liang, L.; Yi, Z.; Li, J.; Xie, X.; Wang, Y.; Li, Y.; Fan, D.; Teh, D. B. L.; All, A. H.; Mohammed, O. F.; Bakr, O. M.; Wu, T.; Bettinelli, M.; Yang, H.; Huang, W.; Liu, X. All-inorganic perovskite nanocrystal scintillators. *Nature* **2018**, *561*, 88−93.

(3) Protesescu, L.; Yakunin, S.; Bodnarchuk, M. I.; Krieg, F.; Caputo, R.; Hendon, C. H.; Yang, R. X.; Walsh, A.; Kovalenko, M. V. Nanocrystals of cesium lead halide perovskites ($CsPbX_3$, X = Cl, Br, and I): Novel optoelectronic materials showing bright emission with wide color gamut. *Nano Lett.* **2015**, *15*, 3692−3696.

(4) Akkerman, Q. A.; Rainó, G.; Kovalenko, M. V.; Manna, L. Genesis, challenges and opportunities for colloidal lead halide perovskite nanocrystals. *Nat. Mater.* **2018**, *17*, 394.

(5) Park, Y.-S.; Guo, S.; Makarov, N. S.; Klimov, V. I. Room temperature single-photon emission from individual perovskite quantum dots. *ACS Nano* **2015**, *9*, 10386−10393.

(6) Yu, B.; Zhang, C.; Chen, L.; Qin, Z.; Huang, X.; Wang, X.; Xiao, M. Ultrafast dynamics of photoexcited carriers in perovskite semiconductor nanocrystals. *Nanophotonics* **2021**, *10*, 1943−1965.

(7) Lin, J.; Gomez, L.; de Weerd, C.; Fujiwara, Y.; Gregorkiewicz, T.; Suenaga, K. Direct observation of band structure modifications in nanocrystals of $CsPbBr_3$ perovskite. *Nano Lett.* **2016**, *16*, 7198.

(8) Becker, M. A.; Vaxenburg, R.; Nedelcu, G.; Sercel, P. C.; Shabaev, A.; Mehl, M. J.; Michopoulos, J. G.; Lambrakos, S. G.; Bernstein, N.; Lyons, J. L.; Stöferle, T.; Mahrt, R. F.; Kovalenko, M. V.; Norris, D. J.; Rainó, G.; Efros, A. L. Bright triplet excitons in caesium lead halide perovskites. *Nature* **2018**, *553*, 189.

(9) Ramade, J.; Andriambariarijaona, L. M.; Steinmetz, V.; Goubet, N.; Legrand, L.; Barisien, T.; Bernardot, F.; Testelin, C.; Lhuillier, E.; Bramati, A.; Chamarro, M. Fine structure of excitons and electron-hole exchange energy in polymorphic $CsPbBr_3$ single nanocrystals. *Nanoscale* **2018**, *10*, 6393−6401.

(10) Tamarat, Ph.; Bodnarchuk, M. I.; Trebbia, J.-B.; Erni, R.; Kovalenko, M. V.; Even, J.; Lounis, B. The ground exciton state of formamidinium lead bromide perovskite nanocrystals is a singlet dark state. *Nat. Mater.* **2019**, *18*, 717−724.

(11) Fu, M.; Tamarat, P.; Huang, H.; Even, J.; Rogach, A. L.; Lounis, B. Neutral and charged exciton fine structure in single lead halide perovskite nanocrystals revealed by magneto-optical spectroscopy. *Nano Lett.* **2017**, *17*, 2895−2901.

(12) Isarov, M.; Tan, L. Z.; Bodnarchuk, M. I.; Kovalenko, M. V.; Rappe, A. M.; Lifshitz, E. Rashba effect in a single colloidal $CsPbBr_3$ perovskite nanocrystal detected by magneto-optical measurements. *Nano Lett.* **2017**, *17*, 5020−5026.

(13) Canneson, D.; Shornikova, E. V.; Yakovlev, D. R.; Rogge, T.; Mitioglu, A. A.; Ballottin, M. V.; Christianen, P. C. M.; Lhuillier, E.; Bayer, M.; Biadala, L. Negatively charged and dark excitons in $CsPbBr_3$ perovskite nanocrystals revealed by high magnetic fields. *Nano Lett.* **2017**, *17*, 6177−6183.

(14) Nestoklon, M. O.; Goupalov, S. V.; Dzhioev, R. I.; Ken, O. S.; Korenev, V. L.; Kusrayev, Yu. G.; Sapega, V. F.; de Weerd, C.; Gomez, L.; Gregorkiewicz, T.; Lin, J.; Suenaga, K.; Fujiwara, Y.; Matyushkin, L. B.; Yassievich, I. N. Optical orientation and alignment of excitons in ensembles of inorganic perovskite nanocrystal. *Phys. Rev. B: Condens. Matter Mater. Phys.* **2018**, *97*, 235304.

(15) Crane, M. J.; Jacoby, L. M.; Cohen, T. A.; Huang, Y.; Luscombe, C. K.; Gamelin, D. R. Coherent spin precession and lifetime-limited spin dephasing in $CsPbBr_3$ perovskite nanocrystals. *Nano Lett.* **2020**, *20*, 8626−8633.

(16) Strohmair, S.; Dey, A.; Tong, Y.; Polavarapu, L.; Bohn, B. J.; Feldmann, J. Spin polarization dynamics of free charge carriers in $CsPbI_3$ nanocrystals. *Nano Lett.* **2020**, *20*, 4724−4730.

(17) Giovanni, D.; Ma, H.; Chua, J.; Grätzel, M.; Ramesh, R.; Mhaisalkar, S.; Mathews, N.; Sum, T. C. Highly spin-polarized carrier dynamics and ultralarge photoinduced magnetization in $CH_3NH_3PbI_3$ perovskite thin films. *Nano Lett.* **2015**, *15*, 1553−1558.

(18) Yu, Z. G. Effective-mass model and magneto-optical properties in hybrid perovskites. *Sci. Rep.* **2016**, *6*, 28576.

(19) Zhang, C.; Sun, D.; Yu, Z.-G.; Sheng, C.-X.; McGill, S.; Semenov, D.; Vardeny, Z. V. Field-induced spin splitting and anomalous photoluminescence circular polarization in $CH_3NH_3PbI_3$ films at high magnetic field. *Phys. Rev. B: Condens. Matter Mater. Phys.* **2018**, *97*, 134412.

(20) Wang, R.; Hu, S.; Yang, X.; Yan, X.; Li, H.; Sheng, C. Circularly polarized photoluminescence and Hanle effect measurements of spin relaxation in organic-inorganic hybrid perovskite films. *J. Mater. Chem. C* **2018**, *6*, 2989−2995.

(21) Hanrahan, M. P.; Men, L.; Rosales, B. A.; Vela, J.; Rossini, A. J. Sensitivity-enhanced ^{207}Pb solid-state NMR spectroscopy for the rapid, non-destructive characterization of organolead halide perovskites. *Chem. Mater.* **2018**, *30*, 7005−7015.

(22) Wang, J.; Zhang, C.; Liu, H.; McLaughlin, R.; Zhai, Y.; Vardeny, S. R.; Liu, X.; McGill, S.; Semenov, D.; Guo, H.; Tsuchikawa, R.; Deshpande, V. V.; Sun, D.; Vardeny, Z. V. Spinoptoelectronic devices based on hybrid organic-inorganic trihalide perovskites. *Nat. Commun.* **2019**, *10*, 129.

(23) Aebli, M.; Piveteau, L.; Nazarenko, O.; Benin, B. M.; Krieg, F.; Verel, R.; Kovalenko, M. V. Lead-halide scalar couplings in ^{207}Pb NMR of $APbX_3$ perovskites (A = Cs, methylammonium, formamidinium; X = Cl, Br, I). *Sci. Rep.* **2020**, *10*, 8229.

(24) Zhou, M.; Sarmiento, J. S.; Fei, C.; Zhang, X.; Wang, H. Effect of composition on the spin relaxation of lead halide perovskites. *J. Phys. Chem. Lett.* **2020**, *11*, 1502−1507.

(25) Mohd Yusoff, A.. R. b.; Mahata, A.; Vasilopoulou, M.; Ullah, H.; Hu, B.; Jose da Silva, W.; Kurt Schneider, F.; Gao, P.; Ievlev, A. V.; Liu, Y.; Ovchinnikova, O. S.; De Angelis, F.; Khaja Nazeeruddin, M. Observation of large Rashba spin-orbit coupling at room temperature in compositionally engineered perovskite single crystals

and application in high performance photodetectors. *Mater. Today* **2021**, *46*, 18−27.
(26) *Semiconductor Spintronics and Quantum Computation*; Awschalom, D. D., Loss, D., Samarth, N., Eds.; Springer: Berlin, 2002.
(27) Yakovlev, D. R.; Bayer, M. Chapter 6. Coherent Spin Dynamics of Carriers. In *Spin Physics in Semiconductors*; Dyakonov, M. I., Ed.; Springer International Publishing AG, 2017; pp 155−206.
(28) Gupta, J. A.; Awschalom, D. D.; Efros, Al. L.; Rodina, A. V. Spin dynamics in semiconductor nanocrystals. *Phys. Rev. B: Condens. Matter Mater. Phys.* **2002**, *66*, 125307.
(29) Fumani, A. K.; Berezovsky, J. Magnetic-field-dependent spin decoherence and dephasing in room-temperature CdSe nanocrystal quantum dots. *Phys. Rev. B: Condens. Matter Mater. Phys.* **2013**, *88*, 155316.
(30) Feng, D. H.; Yakovlev, D. R.; Pavlov, V. V.; Rodina, A. V.; Shornikova, E. V.; Mund, J.; Bayer, M. Dynamic evolution from negative to positive photocharging in colloidal CdS quantum dots. *Nano Lett.* **2017**, *17*, 2844−2851.
(31) Hu, R. R.; Yakovlev, D. R.; Liang, P.; Qiang, G.; Chen, C.; Jia, T. Q.; Sun, Z. R.; Bayer, M.; Feng, D. H. Origin of two Larmor frequencies in the coherent spin dynamics of colloidal CdSe quantum dots revealed by controlled charging. *J. Phys. Chem. Lett.* **2019**, *10*, 3681−3687.
(32) Belykh, V. V.; Yakovlev, D. R.; Glazov, M. M.; Grigoryev, P. S.; Hussain, M.; Rautert, J.; Dirin, D. N.; Kovalenko, M. V.; Bayer, M. Coherent spin dynamics of electrons and holes in $CsPbBr_3$ perovskite crystals. *Nat. Commun.* **2019**, *10*, 673.
(33) Odenthal, P.; Talmadge, W.; Gundlach, N.; Wang, R.; Zhang, C.; Sun, D.; Yu, Z.-G.; Valy Vardeny, Z.; Li, Y. S. Spin-polarized exciton quantum beating in hybrid organic-inorganic perovskites. *Nat. Phys.* **2017**, *13*, 894−899.
(34) Greilich, A.; Oulton, R.; Zhukov, E. A.; Yugova, I. A.; Yakovlev, D. R.; Bayer, M.; Shabaev, A.; Efros, Al. L.; Merkulov, I. A.; Stavarache, V.; Reuter, D.; Wieck, A. Optical control of spin coherence in singly charged (In,Ga)As/GaAs quantum dots. *Phys. Rev. Lett.* **2006**, *96*, 227401.
(35) Yarita, M.; Aharen, T.; Tahara, H.; Saruyama, M.; Kawawaki, T.; Sato, R.; Teranishi, T.; Kanemitsu, Y. Observation of positive and negative trions in organic-inorganic hybrid perovskite nanocrystals. *Phys. Rev. Mater.* **2018**, *2*, 116003.
(36) Nakahara, S.; Tahara, H.; Yumoto, G.; Kawawaki, T.; Saruyama, M.; Sato, R.; Teranishi, T.; Kanemitsu, Y. Suppression of trion formation in $CsPbBr_3$ perovskite nanocrystals by postsynthetic surface modification. *J. Phys. Chem. C* **2018**, *122*, 22188−22193.
(37) Gréboval, C.; Rastogi, P.; Qu, J.; Chu, A.; Ramade, J.; Khalili, A.; Dabard, C.; Dang, T. H.; Cruguel, H.; Ouerghi, A.; Witkowski, N.; Silly, M. G.; Lhuillier, E. Direct observation of the electronic coupling between absorbing and transport layer in quantum dot based solar cell using time resolved photoemission. *J. Phys. Chem. C* **2020**, *124*, 23400.
(38) Mir, W. J.; Livache, C.; Goubet, N.; Martinez, B.; Jagtap, A.; Chu, A.; Coutard, N.; Cruguel, H.; Barisien, T.; Ithurria, S.; Nag, A.; Dubertret, B.; Ouerghi, A.; Silly, M. G.; Lhuillier, E. Strategy to overcome recombination limited photocurrent generation in $CsPbX_3$ nanocrystal arrays. *Appl. Phys. Lett.* **2018**, *112*, 113503.
(39) Zhukov, E. A.; Kirstein, E.; Smirnov, D. S.; Yakovlev, D. R.; Glazov, M. M.; Reuter, D.; Wieck, A. D.; Bayer, M.; Greilich, A. Spin inertia of resident and photoexcited carriers in singly charged quantum dots. *Phys. Rev. B: Condens. Matter Mater. Phys.* **2018**, *98*, No. 121304(R).
(40) Heisterkamp, F.; Zhukov, E. A.; Greilich, A.; Yakovlev, D. R.; Korenev, V. L.; Pawlis, A.; Bayer, M. Longitudinal and transverse spin dynamics of donor-bound electrons in fluorine-doped ZnSe: Spin inertia versus Hanle effect. *Phys. Rev. B: Condens. Matter Mater. Phys.* **2015**, *91*, 235432.
(41) Roth, L. M.; Lax, B.; Zwerdling, S. Theory of optical magneto-absorption effects in semiconductors. *Phys. Rev.* **1959**, *114*, 90.
(42) Yugova, I. A.; Greilich, A.; Yakovlev, D. R.; Kiselev, A. A.; Bayer, M.; Petrov, V. V.; Dolgikh, Yu. K.; Reuter, D.; Wieck, A. D. Universal behavior of the electron *g*-factor in GaAs/AlGaAs quantum wells. *Phys. Rev. B: Condens. Matter Mater. Phys.* **2007**, *75*, 245302.
(43) Belykh, V. V.; Greilich, A.; Yakovlev, D. R.; Yacob, M.; Reithmaier, J. P.; Benyoucef, M.; Bayer, M. Electron and hole *g* factors in InAs/InAlGaAs self-assembled quantum dots emitting at telecom wavelengths. *Phys. Rev. B: Condens. Matter Mater. Phys.* **2015**, *92*, 165307.

https://doi.org/10.1021/acs.nanolett.1c03292
Nano Lett. XXXX, XXX, XXX−XXX